JOURNAL OF MATERIALS SCIENCE 20 (1985) 3967–3975

Fracture toughness of 2-D carbon fibre reinforced carbon composites

H. C. KIM
Physics Department, Korea Advanced Institute of Science and Technology, Chongyangni, PO Box 150, Seoul, Korea

K. J. YOON
Korea Institute of Machinery and Metals, 66 Sang Nam Dong, Changwon, Kyungnam, Korea

R. PICKERING
Royal Ordnance, Explosives Division, Westcott, Aylesbury, Buckinghamshire, UK

P. J. SHERWOOD
Admiralty Research Establishment, Portland, Dorset, UK

The fracture toughness of 2-D woven carbon fibre reinforced carbon laminate has been evaluated by linear elastic fracture mechanics (LEFM), *R*-curve and *J*-integral analysis using the single edge-notched bending (SENB) specimen of edge and flatwise geometries. The edgewise specimens failed by a small extension of the self similar crack whereas the flatwise specimens failed by delamination. The surface damage developing from the tip of the initial crack was revealed by the brittle lacquer coating technique and the zone shape varied with the specimen geometry, i.e. the loading axis relative to the woven layers. Acoustic emission (AE) was also used to monitor crack growth, and the total ring down count of AE was observed to increase as the initial crack length was decreased. Both the damage zone size and total AE counts were found to increase in two linear stages as a function of the square of the stress intensity factor, *K*.

1. Introduction

Woven carbon fibre and more recently, graphite fibre fabrics are attractive for the fabrication of two-dimensional carbon fibre reinforced carbon (CFRC) matrix composites because of their relatively low cost and good drape characteristics for the lay-up of complex shapes. The resistance of CFRC composites to crack propagation is mainly dependent on the nature of the fibre/matrix interface [1]. Although fracture mechanics has been extensively applied to fibre reinforced plastics [2–4] and more recently to polygranular graphites [5], there is little published data [6] on the fracture toughness of CFRC. Another parameter which has frequently been used to compare the toughness of different materials is the fracture surface energy or work of fracture, γ. For materials composed entirely of carbon, γ may vary from 40 to 100 $J\,m^{-2}$ for polygranular graphites to 340 to 1900 $J\,m^{-2}$ for random or 2-D CFRC [7].

In this study the orientation dependence of crack propagation with respect to the laminate direction in three types of 2-D cloth-based CFRCs has been investigated, and the applicability of LEFM, *R*-curve and *J*-integral has been examined. The development of damage zone, size and character has been correlated with acoustic emission and stress intensity factor.

2. Experimental procedure

Flat laminates were fabricated from three commercial grades of woven graphite fibre cloth; A, Hitco G2206 rayon-based satin weave;

TABLE I Specimen size.

	No. 263-Rayon		No. 254 Rayon Plain		No. 266 PAN	
	Edgewise	Flatwise	Edgewise	Flatwise	Edgewise	Flatwise
Span (mm)	70	42	70	42	70	28
Depth (mm)	10	6	10	6	10	4
Thickness (mm)	6	10	6	10	4	10

B, Courtaulds WF 315 PAN-based square weave; C, Le Carbone TGM 389 rayon-based satin weave.

The cloth was pre-impregnated with a mixture of 25 parts by weight Le Carbone EG 3851 graphite powder and 100 parts by weight polyphenylene resin dissolved in MEK to give a nominal 50 wt% fibre fraction. Plates were made by compression moulding and carbonized at 950° C under nitrogen. SENB specimens 80 mm × 10 mm × 6 mm for edgewise geometry and 50 mm × 6 mm × 10 mm for flatwise geometry were cut from the plates with the long axis parallel to the warp direction. Slits were machined in the specimens as shown in Fig. 1 and Table I using a fine slitting wheel to give a slit 0.25 mm wide. The slit depth, a, was varied to give a/W ratios in the range 0.3 to 0.6.

Fracture toughness tests were carried out in three-point bending at room temperature with a span to depth ratio of 7 and a crosshead speed of 0.2 mm min^{-1} in an Instron testing machine. Tests were carried out for both the edge and flatwise loading geometry. Crack propagation during the tests was detected by acoustic emission monitoring using an AET Model 201 (USA) with a total gain of 66 dB and a 175 kHz resonant frequency transducer attached to the notched side of the specimen.

The development of the damage zone at the crack tip with increasing load was recorded photographically using brittle lacquer coatings; Types TL-500-75A and U-10-A, Vishay Intertechnology, USA with oblique illumination.

3. Results and discussion

Typical load–displacement curves for specimens with varying a/W ratio are shown in Figs. 2a to c, where higher maximum loads for small a/W are noticeable for all specimens of both loading geometries. The linearity of load against displacement extended up to 80 to 90% of the maximum load for edgewise geometry specimens, while the flatwise geometry specimens showed a deviation from linearity at 10 to 20% of the maximum load followed by a slow increase of the load with displacement. The larger displacement to failure and a substantial hardening was observed in flatwise geometry of rayon-based Type A and C; however, there was virtually no difference between edge and flatwise specimens of PAN-based Type B. The delamination prevailing in the flatwise specimen at the crack tip blunts the precut crack and absorbs energy, thus causing behaviour similar to work hardening in metals.

3.1. Linear fracture toughness

The stress intensity factors, K_{IC}, at the onset of non-linearity, K_Q, at the crack initiation point defined by ASTM E-399 standard test method, and K_C, at the maximum load were calculated from Equation 1 [8]

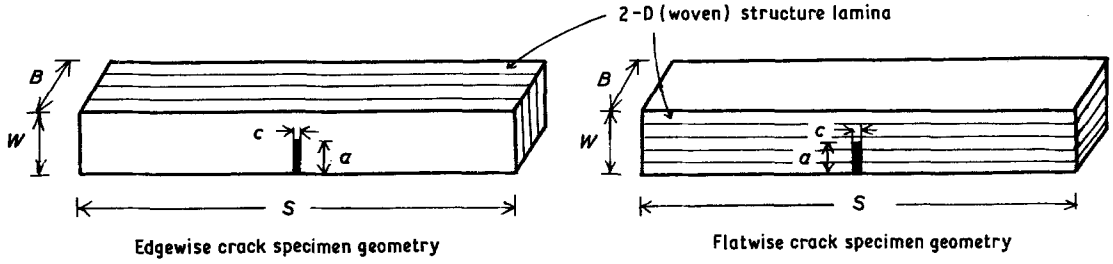

Figure 1 Specimen geometry, S = span, W = specimen depth, B = specimen thickness, a = crack length, c = crack thickness (0.25 mm).

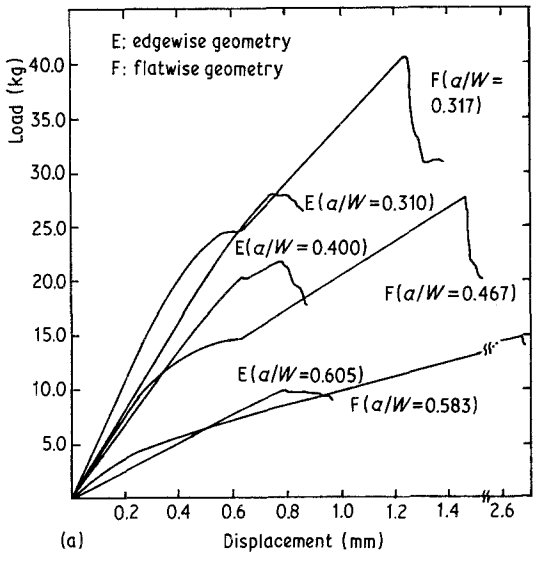

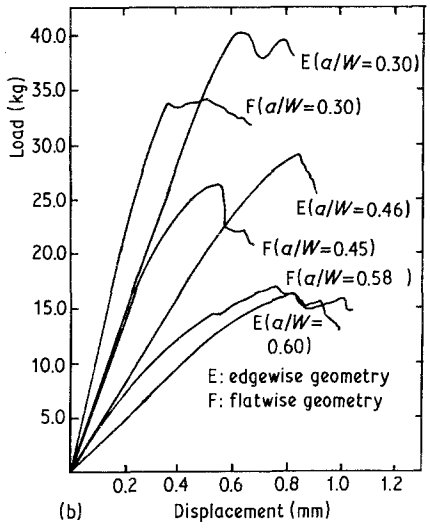

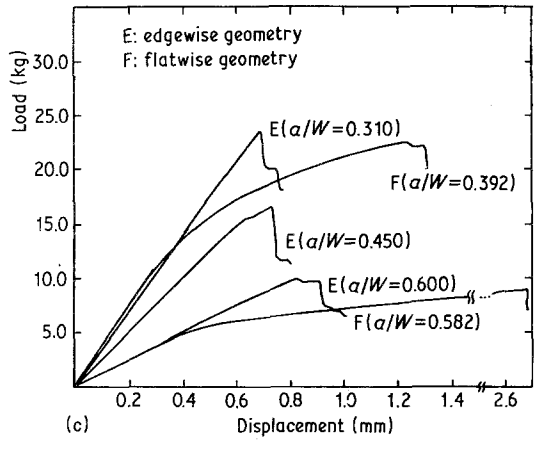

Figure 2 Load–displacement curves for (a) Type A specimens, (b) Type B specimens, and (c) Type C specimens.

$$K = \frac{PS}{BW^{3/2}} Y\left(\frac{a}{W}\right) \quad (1)$$

where

$$Y = \left\{3\left(\frac{a}{W}\right)^{1/2}\left[1.99 - \frac{W}{a}\left(1 - \frac{a}{W}\right) \times \left(2.15 - \frac{3.89}{W}a + 2.7\frac{a^2}{W^2}\right)\right]\right\} \Big/ \left[2\left(1 + \frac{2a}{W}\right)\left(a - \frac{a}{W}\right)^{3/2}\right]$$

where P is the applied load, S is the span, W is the depth, B is the thickness of specimen, and a is the crack length. However, a_{eff}, which is obtained from the compliance curves, was used to calculate K_Q and K_C.

The dependence of stress intensity factors K_{IC}, K_Q and K_C on the a/W ratio for both edge and flatwise geometries is shown in Fig. 3, where it is noticeable that K_{IC} and K_Q for edgewise specimens exceeds that of flatwise specimens, furthermore K_{IC} and K_Q of all specimens regardless of their loading geometry decrease with an increase in a/W ratio.

The application of linear elastic fracture mechanics to carbon/carbon composites [6] and (0°/90°) laminates of CFRP and CFRC [3] has been investigated and it was shown that the critical stress intensity factor, K_C, was independent of a/W ratio providing that failure has coplanar crack propagation. As a result, they were inclined to consider the parameters of LEFM as reasonable material constants.

The main crack in edgwise specimens extended in a colinear direction with respect to precut notch and the stress field around the crack tip is similar to that of Mode I fracture. However, the failure in flatwise specimens was caused by delamination perpendicular to the precut notch, thus a comparison in terms of conventional stress intensity factors is invalid. The variation of stress intensity factors with a/W ratio in the present work indicates that LEFM parameters and approach are not appropriate for the assessment of these types of materials.

3.2. K_R curves

The characteristic resistance of a material to crack extension, K_R, is obtained from

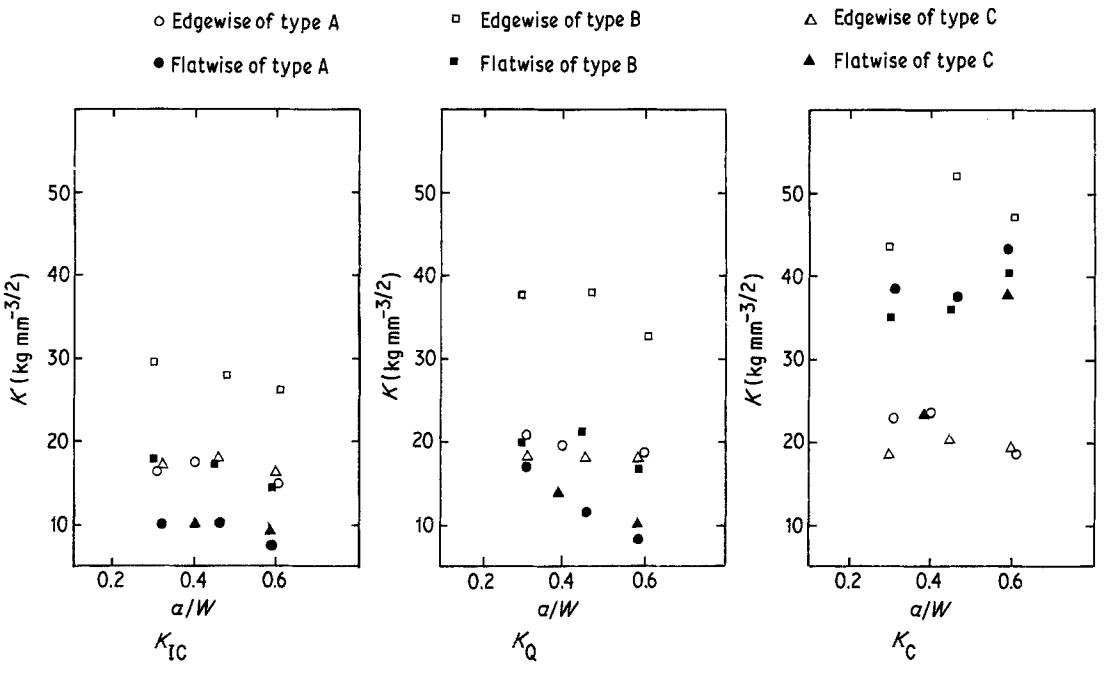

Figure 3 K_{IC}, K_Q, K_C as a function of crack depth ratio, a/W.

Equation 2 [8]

$$K_R = \frac{PS}{BW^{3/2}} Y\left(\frac{a_{eff}}{W}\right) \quad (2)$$

where the notations are the same as in Equation 1 except effective crack length, a_{eff}, which is determined from the corresponding compliance curve. For K_R to qualify as the characteristic resistance of material to crack extension, the shape of the curve should not be altered by initial crack length. It is seen in Fig. 4a that the shapes of the K_R curves are independent of the initial crack length for all edgewise geometry except Type B specimen. In fact, the results of edgewise geometry are this case, which is commonly observed in metallic materials [9] and (0°/90°)2s CFRP [4] beyond G_{IC}.

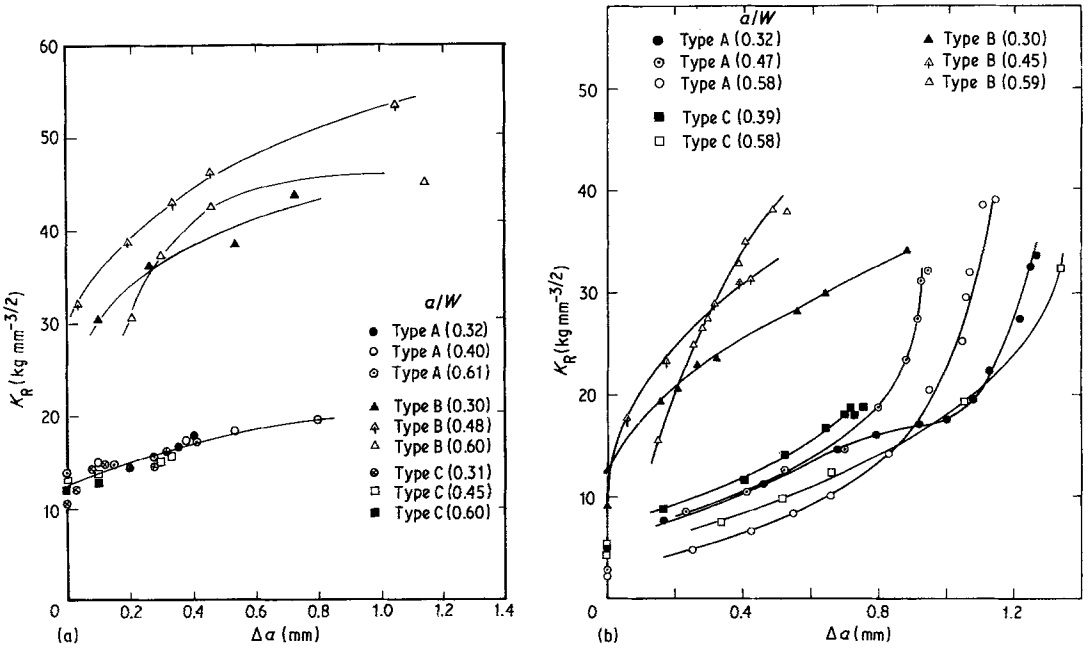

Figure 4 K_R curves for (a) edgewise geometry, (b) flatwise geometry.

In contrast, two modes of variation of K_R with Δa were observed for the flatwise geometry of Type A and C. The fibre restrains crack extension to the colinear direction at the tip of initial crack, instead delamination tends to extend perpendicular to the initial crack by slow stable crack growth which causes K_R to increase rapidly with Δa, while the specimen undergoes substantial "hardening" as seen in Figs. 2a to c.

Similarly two stages of variation or multiple serration in the K_R curves was reported by Antolovich *et al.* [10], in a composite of tough maraging steel fibres embedded in a brittle maraging steel matrix, which was attributed to debonding between the fibres and matrix. Consequently, they suggested that a single fracture mechanics parameter cannot adequately describe crack extension in such highly directional composites. Furthermore, the K_R curves obtained by Ochai and Peters [4] for centre notched $(0°/90°)2s$ and $(0°/\pm 45\%)s$ CFRP laminates showed a large scatter with no obvious trend as a function of $2a/W$ over the range 0.14 to 0.51.

The K_R curves of the present work, except edgewise geometry of Type A and C, tend to vary with a/W ratio contrary to the K_R curve concept of invariant crack growth resistance with initial crack length.

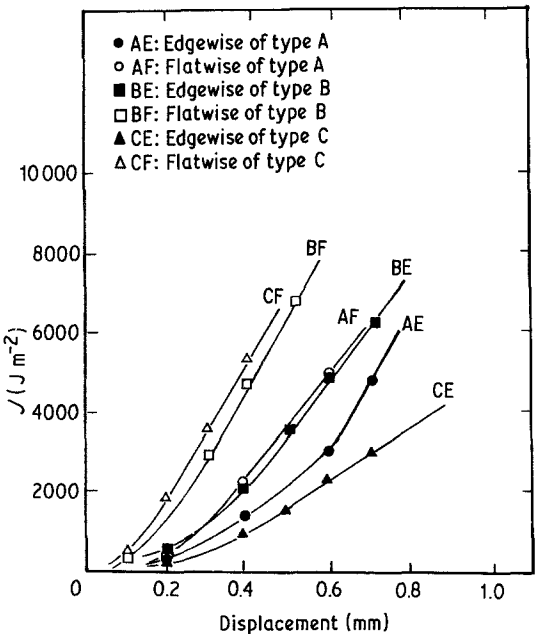

Figure 5 J–displacement curves for the specimens.

3.3. J-integral

As shown in Figs. 2a to c, the load–displacement curves of both specimen orientations showed a substantial non-linear region, especially the flatwise orientation. The preceding LEFM and R-curve analyses have been shown to be only partially valid for CFRC, and the same experimental results have been used to examine the validity of the J-integral parameter to these composites using the method described by Begley and Landes [11]

$$J = -\frac{1}{B}\left(\frac{dU}{da}\right) \tag{3}$$

where U is the observed energy, B is the specimen thickness and a is the initial crack length. Fig. 5 shows J-integral against displacement of all specimens tested in both edge and flatwise geometries, where one can observed two stages of variation with the displacement.

It was observed that the flatwise geometry of all three specimen types had lower critical displacements and larger J values than the edgewise geometry. As discussed in Section 3.2, the blunting followed by delamination and subsequent work hardening of the three-point bending beam with reduced depth may be attributable to the higher energy required for unit crack extension. The merit of the J-integral analysis is that the ambiguity of the criterion arising from variation with a/W ratio and mode of failure disappears in this approach.

3.4. Acoustic emission

For the edgewise specimens, the variation of total ring down AE counts with displacement is shown in Fig. 6 together with the corresponding load–displacement curves. It can be seen that N increases in two distinct stages, the first stage corresponding to the linear part and the second stage to the non-linear part of the load–displacement curve. These two stages of AE release are thought to correspond to different events around the crack tip, i.e. the first stage to low energy events such as matrix cracking, interfacial debonding and delamination and the second stage to more energetic events such as fibre fracture. This two-stage variation is in contrast to the work of Carlsson and Norrbom [12].

Fig. 7 summarizes the starting displacement and transition displacement of acoustic emission from the first to second stage as a function of

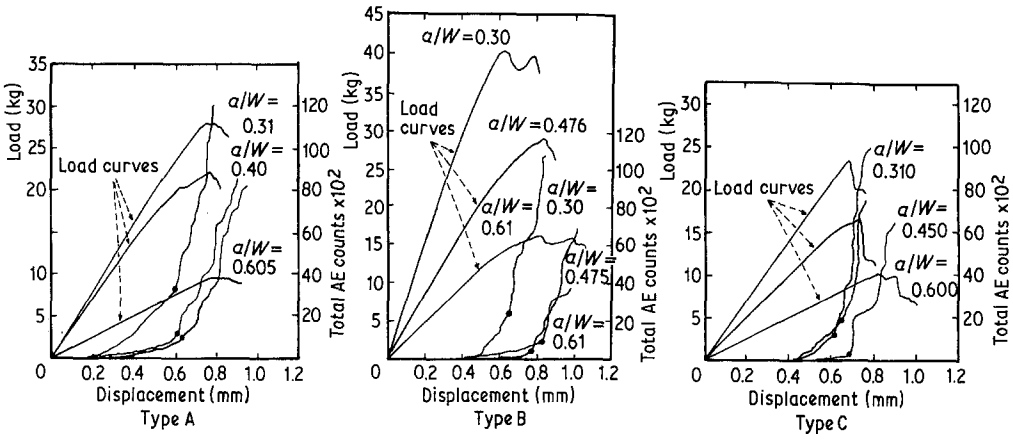

Figure 6 Total acoustic emission counts and load–displacement for the specimen.

a/W ratio, where the transition displacement increased as a/W ratio increased, while the starting displacement remained constant for Types A and C.

3.5. Damage zone revealed by brittle lacquer technique

In fibre composites, the crack tip damage zone may be considered analogous to the plastic zone observed in metals where the local stress field varies with $(r)^{-1/2}$ in LEFM. This suggests that plastic yielding occurring at a critical value of stress should extend to a distance r from the crack tip [13].

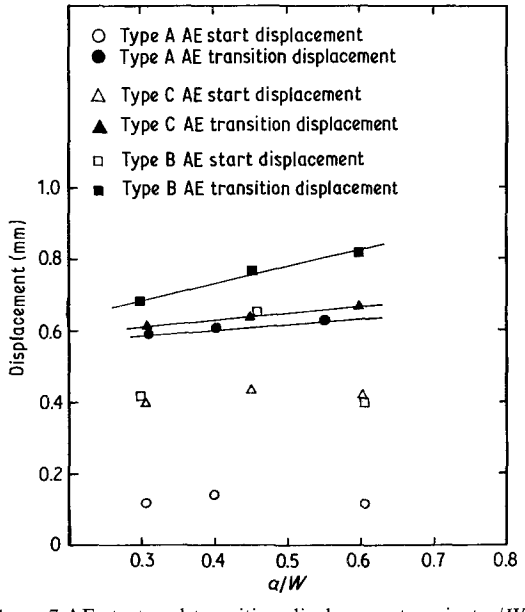

Figure 7 AE start and transition displacement against a/W for edgewise geometry.

$$r \propto \frac{K_I^2}{\sigma_0}$$

where σ_0 is the effective yield stress.

The change in fibre composition and loading mode such as edge and flatwise, will affect interlaminar shear strength and compliance. The results in Figs. 8a and b are partly in agreement with such a relationship.

Crack tip blunting takes place as soon as the composites are loaded, similar to the stretched zone in metallic materials, then a narrow damage zone is formed co-directional with the fibres and sub-cracking parallel to the fibres of each ply or delamination between plies occurs.

The brittle lacquer technique is based on the perfect adhesion of a coating with brittle characteristics to the component being studied, and the applied stress transmitted to the coating ultimately causes the coating to fail by cracking perpendicular to the principal strain direction. Since the coating is usually thin relative to the specimen thickness, it is valid to assume that the surface strains occurring in the specimen are transmitted to the coating without attenuation. Determination of the damage zone size requires special techniques due to opacity of CFRC. Previous workers [4, 14] loaded the specimens to a predetermined value of K^2 and on reducing the load 50%, stained the specimen with a fluorescent dye. After unloading completely the damage zone is observed by microscope [14] or X-ray [4] but these techniques cannot be used for *in situ* measurements.

In the present work the isostatic contour line of lacquer cracking at the tip of the pre-cut notch was observed, and the area of lacquer cracking was taken as the extent of the surface

(a)

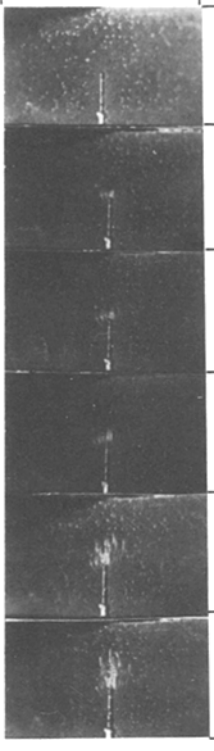

Damage zone (mm^3)	P (load) kg	K ($kg\,mm^{-3/2}$)	K^2 ($kg\,mm^{-3/2})^2$
0	5.6	4.71	22.18
8.3	10.3	8.67	75.17
15.2	14.2	11.95	142.78
21.5	15.9	14.20	201.64
33.7	16.7	15.52	240.87
40.5	9.0		

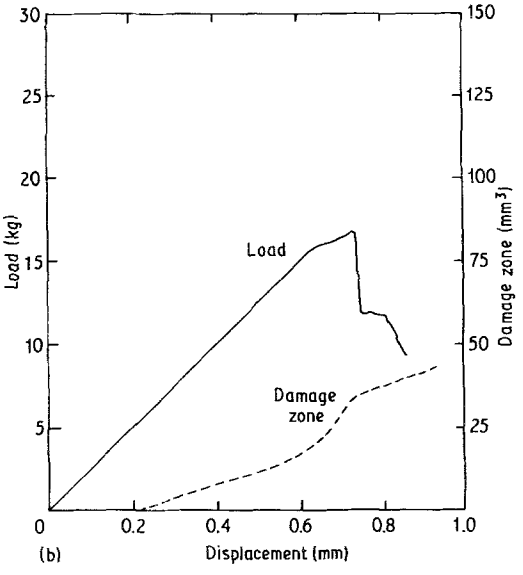

(c)

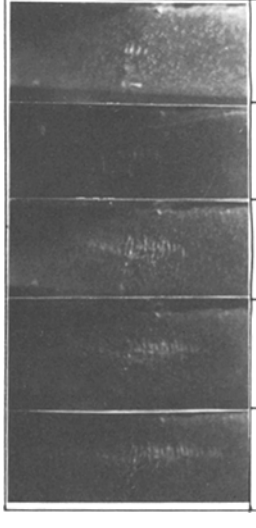

Damage zone (mm^3)	P (load) kg	K ($kg\,mm^{-3/2}$)	K^2
14.7	7.0	4.81	23.18
42.5	11.5	9.31	86.75
123.7	14.4	13.85	191.77
178.6	17.9	20.83	433.76
225.9	20.1	25.62	656.46

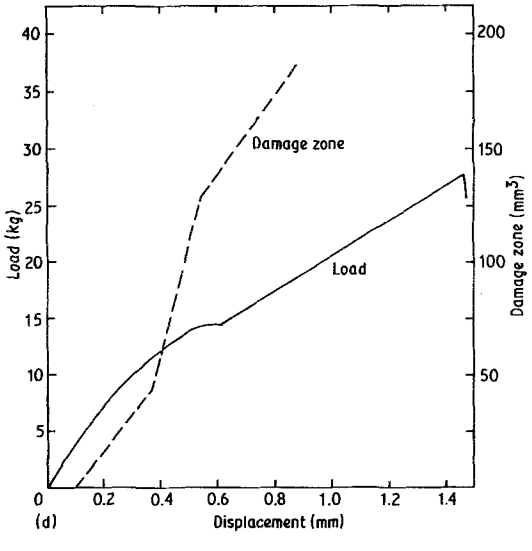

Figure 8 (a) Crack tip damage revealed by the brittle lacquer technique for edgewise geometry ($a/W = 0.45$). (b) Damage zone and load–displacement for Type C edgewise crack specimens ($a/W = 0.45$). (c) Crack tip damage revealed by the brittle lacquer technique for flatwise geometry ($a/W = 0.467$). (d) Damage zone and load–displacement for Type A flatwise crack specimens ($a/W = 0.467$). (e) Damage zone and AE against K^2 for Type C edgewise geometry and Type A flatwise geometry.

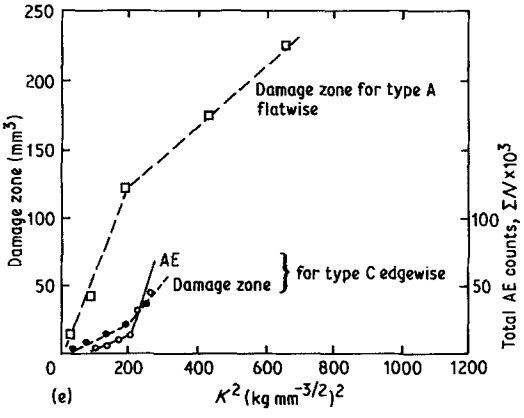

Figure 8 Continued.

damage zone. The bulk damage zone was assumed to be proportional to the product of surface damage zone and the specimen thickness.

Figs. 8a to d show the growth of the damage zone and damage zone against displacement superimposed on to load–displacement curves of edgewise and flatwise geometries. For edgewise specimens the main crack extended colinearly with the precut notch direction and the crack tip stress distribution is similar to that of mode I, consequently the damage zone shape is similar to the plastic zone in isotropic materials. For the flatwise geometry the crack extended by delamination perpendicular to precut notch direction, as discussed in Section 3.2 for K_R curves, the loading condition in the delaminated region is similar to that of a beam in three-point bending in which the cross-section is the remaining section above delamination of the specimen, hence the stress system is no longer mode I. The lacquer cracking lines in this delaminated region are observed perpendicular to lamina direction, and the length of lacquer cracking decreases as the region is further away from precut crack since the bending tensile stress decreases from the mid-point of the span. Thus in the flatwise geometry we observe that the damage zone is caused mainly by tensile bending stress at the mid-region of remaining cross-section rather than crack tip stress concentration.

The damage zone, as shown in Figs. 8b and d increased linearly with displacement; however, it is apparent that the linearity deviates around the onset of permanent deformation on the load–displacement curve, corresponding to a rapid growth of the damage zone.

A region of stable crack growth at the tip of the main crack or notch consisting of sub-critical cracking parallel to the fibres of each ply and delaminations between plies has been considered as a damage zone in the composites by Mandell *et al.* [14] using staining with fluorescent dye technique for (90°/0°)s, (45°/−45°)s, (30°/−30°)s and (15°/15°)s CFRP lamainates and they observed a proportionality between the subcrack length and K^2 for notch sensitive laminates. Recently, Ochai and Peters [4] used an X-ray technique to reveal the damage zone in the centre notched (0/90°)2s CFRP laminates, but the proportionality between the subcrack length and K^2 was not found. Fig. 8e shows the variation of damage zone and AE against K^2 for Type C edgewise and Type A flatwise specimens in which an almost linear relationship can be observed between the extent of damage zone, AE and K^2, but at the onset of linearity on the load–displacement curves of edgewise geometry due to abrupt increase; while in flatwise geometry damage zone growth slows down at 200 $(\text{kg mm}^{-3/2})^2 K^2$ value less than initial growth rate. The size of the damage zone is characterized by the length of the subcrack in each ply and the extent of any delamination zone between piles. The damage zone is thought to be closely related to the crack propagation resistance of composites with a larger damage zone leading to a higher value of fracture toughness. This interpretation can explain the higher J value for flatwise geometry and higher K_R for flatwise geometry of Types A and C at later stages.

4. Conclusions

1. The fracture toughness parameters are found to depend strongly on the type of carbon fibre cloth used (i.e. PAN or rayon-based) and on the orientation of the initial crack to the cloth layers. When the crack propagation direction was normal to the laminate plane (flatwise), severe crack blunting and delamination occurred rendering the results invalid. However, when the crack propagation direction was in the laminate plane (edgewise) fracture occurred colinear with the initial crack (Mode I) and valid facture toughness parameters could be measured.

2. For the CFRC materials used in this work, the stress intensity factors K_{IC}, K_C and K_Q were found to be dependent on a/W ratio for values up to 0.6. Hence a simple LEFM analysis is not considered appropriate.

3. Crack growth resistance (K_R) curves were found to depend on the orientation of the initial crack and on the value of a/W. K_R cannot, therefore, be considered as an intrinsic property of these materials.

4. The J-integral was found to be the most appropriate fracture mechanism parameter for this type of material (brittle fibre–brittle matrix with low fibre/matrix bonding).

5. Both the damage zone size revealed by the brittle lacquer technique and the total counts of acoustic emission were found to increase in two linear stages as a function of K^2. These two stages are believed to be associated with different micromechanisms of crack propagation, the first fibre/matrix debonding and matrix cracking, and the second fibre fracture.

Acknowledgement

This work has been carried out with the support of Procurement Executive, Ministry of Defence, UK. Copyright © Controller, HMSO, London.

References

1. C. R. THOMAS and E. J. WALKER, Proceedings of the 5th London International Carbon Conference, 1978 (Society of Chemical Industry) p. 520.
2. D. C. PHILLIPS and A. S. TELELMAN, *Composites* (September 1972) 216.
3. D. C. PHILLIPS, *J. Compos. Mater.* **8** (1974) 130.
4. S. OCHAI and O. W. N. PETERS, *J. Mater. Sci.* **17** (1982) 417.
5. M. RODIG, G. KLEIST, H. SCHIFFERS and H. NICKEL, Proceedings of the 5th London International Carbon Conference, 1978 (Society of Chemical Industry) p. 51.
6. T. R. GUESS and W. R. HOOVER, *J. Compos. Mater.* **7** (1973) 2.
7. J. X. ZHAO, R. C. BRADT and P. L. WALKER, 15th Biennial Carbon Conference, USA, 1981, p. 274.
8. J. E. SRAWLEY, *Int. J. Fract.* **12** (1976) 475.
9. "Recommended Practice for R-curve Determination" ASTM Annual Book of Standards. Part 10 (American Society for Testing and Materials, Philadelphia, 1975).
10. S. D. ANTOLOVICH, K. KASI and G. K. CHANANI, ASTM STP 514 (1972) pp. 114 34.
11. J. A. BEGLEY and J. D. LANDES, Proceedings of the 1971 National Symposium on Fracture Mechanics, ASTM STP 514 (1972) pp. 1–20.
12. L. CARLSSON and B. NORRBOM, *J. Mater. Sci.* **18** (1983) 2503.
13. D. BROEK, "Elementary Engineering Fracture Mechanics" (Sijthoff and Nordhoff, 1978) p. 115.
14. J. F. MANDELL, S. S. WANG and F. J. McGARRY, *J. Compos. Mater.* **9** (1975) 266.

Received 1 November
and accepted 28 November 1984